Role of the Low-Affinity Binding Site in Electron Transfer from Cytochrome *c* to Cytochrome *c* Peroxidase†

Hongkang Mei,‡ Lois Geren,‡ Mark A. Miller,§ Bill Durham,‡ and Francis Millett*,‡

Department of Chemistry and Biochemistry, University of Arkansas, Fayetteville, Arkansas 72701, and Joint Center for Structural Genomics, San Diego Supercomputer Center, 9500 Gilman Drive, La Jolla, California 92093-0527

Received December 10, 2001; Revised Manuscript Received January 26, 2002

ABSTRACT: The interaction of yeast iso-1-cytochrome *c* (yCc) with the high- and low-affinity binding sites on cytochrome *c* peroxidase compound I (CMPI) was studied by stopped-flow spectroscopy. When 3 μM reduced yCc^{II} was mixed with 0.5 μM CMPI at 10 mM ionic strength, the Trp-191 radical cation was reduced from the high-affinity site with an apparent rate constant >3000 s^{-1}, followed by slow reduction of the oxyferryl heme with a rate constant of only 10 s^{-1}. In contrast, mixing 3 μM reduced yCc^{II} with 0.5 μM preformed CMPI·yCc^{III} complex led to reduction of the radical cation with a rate constant of 10 s^{-1}, followed by reduction of the oxyferryl heme in compound II with the same rate constant. The rate constants for reduction of the radical cation and the oxyferryl heme both increased with increasing concentrations of yCc^{II} and remained equal to each other. These results are consistent with a mechanism in which both the Trp-191 radical cation and the oxyferryl heme are reduced by yCc^{II} in the high-affinity binding site, and the reaction is rate-limited by product dissociation of yCc^{III} from the high-affinity site with apparent rate constant k_d. Binding yCc^{II} to the low-affinity site is proposed to increase the rate constant for dissociation of yCc^{III} from the high-affinity site in a substrate-assisted product dissociation mechanism. The value of k_d is <5 s^{-1} for the 1:1 complex and >2000 s^{-1} for the 2:1 complex at 10 mM ionic strength. The reaction of horse Cc^{II} with CMPI was greatly inhibited by binding 1 equiv of yCc^{III} to the high-affinity site, providing evidence that reduction of the oxyferryl heme involves electron transfer from the high-affinity binding site rather than the low-affinity site. The effects of CcP surface mutations on the dissociation rate constant indicate that the high-affinity binding site used for the reaction in solution is the same as the one identified in the yCc·CcP crystal structure.

Electron transfer between metalloproteins may depend on many different factors, including the kinetics of complex formation and dissociation, the distance and pathway between the two redox centers in the complex, and the driving force and reorganization energy (*1*−*3*). The reaction between cytochrome *c* (Cc)[1] and cytochrome *c* peroxidase (CcP) has become an important prototype for studying these factors because of the extensive spectroscopic and structural characterization of the individual proteins as well as their 1:1 complex (*4*, *5*). The reaction of hydrogen peroxide with the resting ferric form of CcP leads to the formation of CMPI-(Fe^{IV}=O,$R^{\bullet+}$), which contains an oxyferryl heme Fe^{IV}=O and a radical cation, $R^{\bullet+}$, located on the indole ring of Trp-191 (*6*−*12*). Extensive studies using the ruthenium photoreduction technique as well as stopped-flow spectroscopy have demonstrated that ferrocytochrome *c* initially reduces the Trp-191 radical cation in CMPI(Fe^{IV}=O,$R^{\bullet+}$) under all conditions of ionic strength and pH (*13*−*21*). A second molecule of Cc^{II} then reduces the oxyferryl heme in CMPII(Fe^{IV}=O,R) to form the resting enzyme, as shown in Scheme 1. Earlier studies (*22*−*24*) have also been found to be consistent with initial reduction of the radical cation in CMPI (*19*). The rate constant for electron transfer from Cc^{II} to the radical cation in the physiological yCc·CcO complex (k_{eta}) was found to be 2×10^6 s^{-1} using yeast Ru-39-Cc, which is labeled with ruthenium on the back surface where it does not interfere in the reaction (*19*). The rate constant k_{etb} for electron transfer to the oxyferryl heme was found to be 5000 s^{-1} using the same technique (*19*). Mutagenesis studies demonstrated that yCc used the high-affinity binding site identified in the yCc·CcP crystal structure (*4*) for electron transfer to both the Trp-191 radical cation and the oxyferryl heme (*17*, *19*−*21*). A mechanism was proposed for reduction of the oxyferryl heme

Scheme 1

$$\mathrm{I} + \mathrm{Cc^{II}} \underset{k_d}{\overset{k_f}{\rightleftarrows}} \mathrm{I{:}Cc^{II}} \xrightarrow{k_{eta}} \mathrm{II{:}Cc^{III}} \underset{k_f}{\overset{k_d}{\rightleftarrows}} \mathrm{II} + \mathrm{Cc^{III}}$$

$$\mathrm{II} + \mathrm{Cc^{II}} \underset{k_d}{\overset{k_f}{\rightleftarrows}} \mathrm{II{:}Cc^{II}} \xrightarrow{k_{etb}} \mathrm{E{:}Cc^{III}} \underset{k_f}{\overset{k_d}{\rightleftarrows}} \mathrm{E} + \mathrm{Cc^{III}}$$

† This work was supported in part by NIH Grant GM20488 and NIH NCRR COBRE Grant 1 P20 RR15569.

* To whom correspondence should be addressed. Phone: 501-575-4999. Fax: 501-575-4049. E-mail: millett@uark.edu.

‡ University of Arkansas.

§ San Diego Supercomputer Center.

[1] Abbreviations: Cc, cytochrome *c*; hCc, horse Cc; yCc, yeast iso-1-Cc; CcP, cytochrome *c* peroxidase; CcP(MI), recombinant CcP; CMPI or I, CcP compound I; CMPII or II, CcP compound II; Ru-39-Cc, Ru(bipyridine)$_2$[4,4′-dimethylbipyridine-Cys-39-(H39C,C102T)-yCc].

10.1021/bi016020a CCC: $22.00
Published on Web 02/28/2002

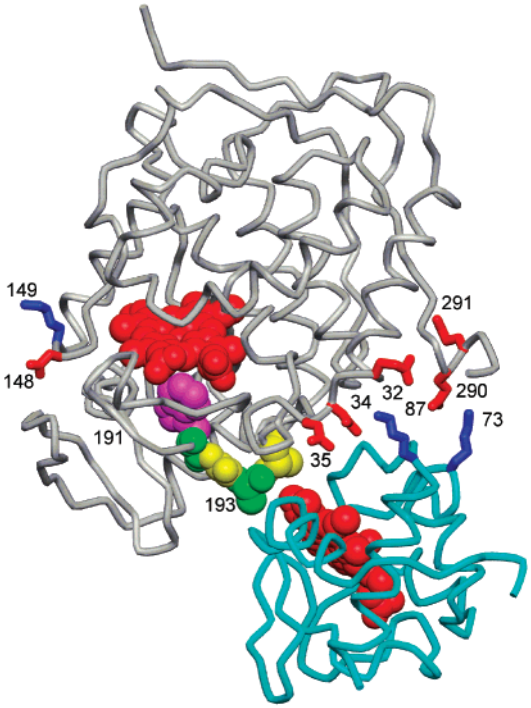

FIGURE 1: X-ray crystal structure of the CcP·yCc complex (*4*). The heme groups are shown in red CPK models, the Trp-191 indole group is in purple, the Trp-191 backbone and Ala-193 are in green, and Gly-192 and Ala 194 are in yellow. The side chains of CcP residues E32, D34, E35, E290, and E291 and yCc residues K73 and K87 are labeled. The low-affinity Cc binding site is proposed to be located near D148 and K149, which are labeled (*34*).

in which internal electron transfer in CMPII(Fe^{IV}═O,R) leads to regeneration of the radical cation in CMPII(Fe^{III},$R^{•+}$), which is then reduced by yCc^{II} (*18*, *19*). Therefore, both reduction steps use the electron-transfer pathway identified in the crystal structure, which extends from the yCc heme methyl group through CcP residues Ala-194, Ala-193, and Gly-192 to the indole group of Trp-191, which is in van der Waals contact with the CcP heme group (Figure 1) (*4*).

Kang et al. (*25*) and Kornblatt and English (*26*) have shown that once Cc has bound to CcP at the high-affinity site to form a 1:1 complex, a second molecule of Cc can bind to a low-affinity site to form a 2:1 complex. The binding of Cc to the low-affinity site affects both the steady-state and stopped-flow kinetics at low ionic strength (*21*, *22*, *27*−*29*). However, two distinctly different mechanisms have been proposed for the role of the low-affinity site. Using the ruthenium photoreduction method, Mei et al. (*20*) reported evidence consistent with a mechanism in which yCc^{II} binding to the low-affinity site significantly increases product dissociation from the high-affinity site, but in which the low-affinity site is not active in direct electron transfer to either the radical cation or the oxyferryl heme. In contrast, Hoffman and co-workers found that the low-affinity binding site is active in electron transfer in 2:1 complexes between Zn-porphyrin-hCc and ferric CcP (*30*−*34*) and between yCc and Zn-porphyrin-CcP (*35*). On this basis they suggested that the low-affinity site may also be active in electron transfer to the physiological oxyferryl heme (*33*, *35*). This question has taken on added importance with recent evidence suggesting that the low-affinity binding site may be located near Asp-148 on CcP (Figure 1) (*34*).

In the present paper the reaction of native yCc^{II} with a preformed 1:1 CMPI·yCc^{III} complex is investigated using stopped-flow spectroscopy. The results are consistent with a mechanism in which dissociation of yCc^{III} from the high-affinity site is very slow and rate-limiting at low ionic strength, and binding yCc^{II} to the low-affinity site significantly increases the rate of product dissociation from the high-affinity site. The reaction of horse Cc^{II} with CMPI was greatly inhibited by binding 1 equiv of yCc^{III} to the high-affinity site, providing evidence that reduction of the oxyferryl heme involves electron transfer from the high-affinity binding site rather than the low-affinity site. The reaction kinetics were the same for wild-type yeast CcP and recombinant CcP(MI), indicating that the sequence variations present in CcP(MI), D152G and T53I (*36*), do not affect the interaction of yCc with the low-affinity site.

EXPERIMENTAL PROCEDURES

Materials. Yeast iso-1-Cc was obtained from Sigma Chemicals Co. and purified as described by Miller et al. (*17*). Cytochrome *c* peroxidase was prepared from Red Star bakers' yeast as described by Geren et al. (*13*). Recombinant CcP(MI) and the mutants E32Q, D34N, E35N, E290N, E291Q, and A193F were prepared as described by Fishel et al. (*37*) and Miller et al. (*17*).

Stopped-Flow Spectroscopy. The reaction between yCc^{II} or hCc^{II} and CMPI was studied using a Hi-Tech SF-61 stopped-flow spectrophotometer equipped with a 1 cm flow cell (*19*). The mixing time of the instrument is 2 ms, limiting the maximum measurable first-order rate constant to about 350 s^{-1} in order to resolve more than 50% of the absorbance change. Wild-type yCc or hCc was reduced with excess ascorbate and dithiothreitiol, passed through a 1 × 30 cm Bio-Gel P-2 column equilibrated with 2 mM sodium phosphate, pH 7.0, and 50 mM NaCl to remove excess reagent, and stored under nitrogen. Precautions were taken to ensure that no H_2O_2 was present in the sample (*19*). One equivalent of H_2O_2 was added to CcP, and the visible spectrum was recorded to measure the formation of CMPI. Cc^{II} and CMPI, each in 5 mM sodium phosphate, pH 7.0, were placed in the two syringes of the stopped-flow apparatus, and transients were recorded within 1 min of CMPI formation. Solutions were then removed from the syringes, and visible spectra were recorded to determine that Cc^{II} and CMPI remained stable. Experiments with the preformed CMPI·yCc^{III} complex were performed in the same fashion except that equimolar yCc^{III} was present in the syringe with CMPI.

The reaction between yCc^{II} and CMPI was monitored at 419 and 434 nm. The 419 nm transient has contributions from the oxidation of yCc^{II} as well as the reduction of the oxyferryl heme in CMPII. The 434 nm transient only has contributions from the reduction of the oxyferryl heme, since 434 nm is an isobestic point for yCc. The reduction of the Trp-191 radical cation makes very little contribution to the absorbance transient at either wavelength. The experimental transients were fit to a single exponential to obtain approximate k_{obs} values. However, it was not possible to obtain exact algebraic solutions to the kinetic mechanisms shown in Schemes 1 and 2. Therefore, numerical integration methods were used to fit the experimental 419 and 434 nm

Scheme 2

$$I{:}Cc^{III} \underset{k_f}{\overset{k_d}{\rightleftarrows}} I + Cc^{III}$$

$$I + Cc^{II} \underset{k_d}{\overset{k_f}{\rightleftarrows}} I{:}Cc^{II} \xrightarrow{k_{eta}} II{:}Cc^{III} \underset{k_f}{\overset{k_d}{\rightleftarrows}} II + Cc^{III}$$

$$II + Cc^{II} \underset{k_d}{\overset{k_f}{\rightleftarrows}} II{:}Cc^{II} \xrightarrow{k_{etb}} E{:}Cc^{III} \underset{k_f}{\overset{k_d}{\rightleftarrows}} E + Cc^{III}$$

transients with the kinetic mechanism, as described in refs *19* and *20*. The absorbance transients at 419 and 434 nm were calculated from the equations:

$$\Delta A_{419} = \Delta\epsilon_{419}[yCc^{II}]_t + \Delta\epsilon'_{419}([I]_t + [II]_t)$$

$$\Delta A_{434} = \Delta\epsilon_{434}([I]_t + [II]_t)$$

where $\Delta\epsilon_{419} = 44$ mM^{-1} cm^{-1} is the extinction coefficient for oxidation of yCc^{II} (*38*) and $\Delta\epsilon'_{419} = 27$ mM^{-1} cm^{-1} and $\Delta\epsilon_{434} = 27$ mM^{-1} cm^{-1} are the extinction coefficients for reduction of the oxyferryl heme in I and II (*39*, *40*). $[yCc^{II}]_t$, $[I]_t$, and $[II]_t$ are the total concentrations of all forms of these compounds, both complexed and uncomplexed. The numerical integration simulations were simultaneously fitted to the experimental 419 and 434 nm transients to obtain the best fits. The fits shown in Figures 3−6 were obtained by adjusting the value of k_d alone. The values of k_f, k_{eta}, and k_{etb} did not affect the fits provided that they were larger than the values given in the text. The k_d values obtained from the numerical integration simulations were then fitted to eqs 1 or 2 using the Marquardt−Levenberg nonlinear regression algorithm in SigmaPlot. The error for each parameter reported is the asymptotic standard error representing 95% confidence limits given by the algorithm.

RESULTS

Reaction of yCc^{II} with CMPI and the CMPI·yCc^{III} Complex at Low Ionic Strength. Previous studies have established that the reaction between yCc^{II} and equimolar CMPI at low ionic strength involves initial reduction of the Trp-191 radical cation in a reaction that is too fast to resolve in the stopped-flow spectrophotometer (*19*). For example, only 15% of the theoretical amplitude was resolved in the 419 nm transient for the reaction between 0.4 μM yCc^{II} and 0.6 μM CMPI at 10 mM ionic strength (Figure 2). The observed rate constant was estimated to be greater than 3000 s^{-1}, and the second-order rate constant was estimated to be greater than 7×10^9 s^{-1}. No transient at all was observed at 434 nm, a Cc isobestic point, consistent with reduction of the Trp-191 radical cation rather than the oxyferryl heme. When 1.1 μM yCc^{II} was mixed with 0.4 μM CMPI, very slow transients were observed at both 419 and 434 nm, with approximate k_{obs} values of 3.5 s^{-1} each (Figure 3). The amplitude of the 419 nm transient accounted for reduction of 0.4 μM CMPII by 0.4 μM yCc^{II}, while the 434 nm transient accounted for

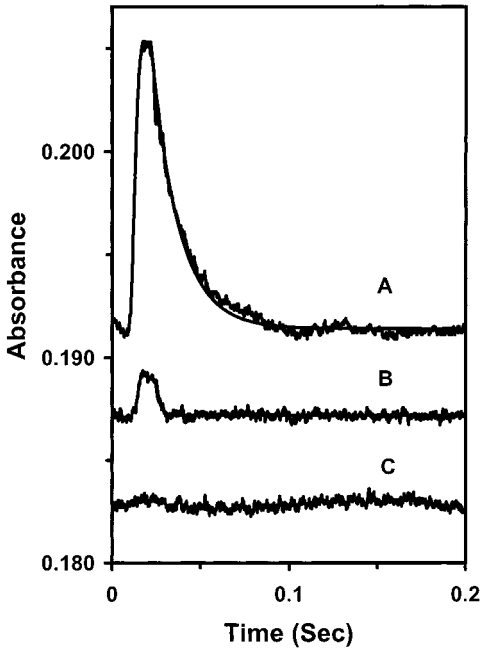

FIGURE 2: Reaction of yCc^{II} with the radical cation in CMPI. The reaction between 0.4 μM yCc^{II} and 0.6 μM CMPI was carried out in 5 mM sodium phosphate, pH 7.0, and 0−300 mM NaCl at 22 °C. (A) 419 nm transient at 310 mM ionic strength. The value of k_{obs} is 65 s^{-1}, and 90% of the theoretical amplitude is observed. (B) 419 nm transient at 10 mM ionic strength. The value of k_{obs} is >3000 s^{-1}, and 15% of the theoretical amplitude is observed. (C) 434 nm transient under the same conditions as in (B).

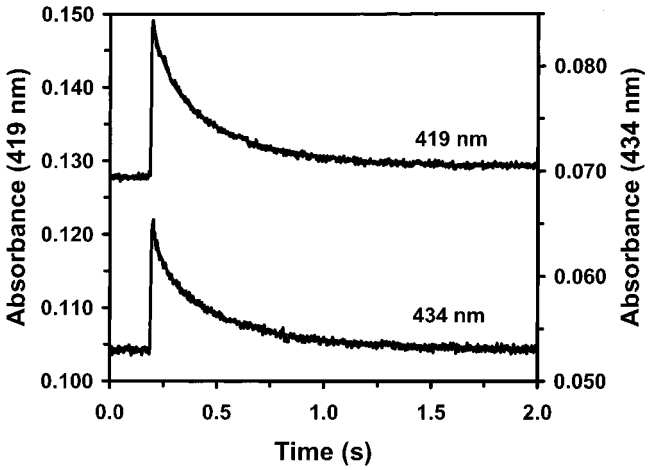

FIGURE 3: Reaction between 1.1 μM yCc^{II} and 0.4 μM CMPI in 5 mM sodium phosphate, pH 7.0, at 22 °C. The solid curves are the best fits of the 419 and 434 nm transients to Scheme 1 with $k_d = 4.7 \pm 0.8$ s^{-1}.

reduction of 0.4 μM CMPII. This indicates that yCc^{II} initially reduced the radical cation in CMPI in a reaction that was too fast to resolve in the stopped-flow spectrophotometer, and then a second molecule of yCc^{II} reduced the oxyferryl heme in CMPII in a very slow reaction. Since the oxyferryl heme is reduced very rapidly by yCc^{II} in the high-affinity site at low ionic strength (*19*), it was postulated that the slow reduction of CMPII in the stopped-flow experiment was rate-limited by the dissociation of yCc^{III} from CMPII. This was confirmed by reacting 0.4 μM yCc^{II} with a preformed complex between 0.5 μM CMPI and 0.5 μM yCc^{III} at 10 mM ionic strength (Figure 4). A very slow 419 nm transient was observed with a k_{obs} of 3.5 s^{-1} and an amplitude

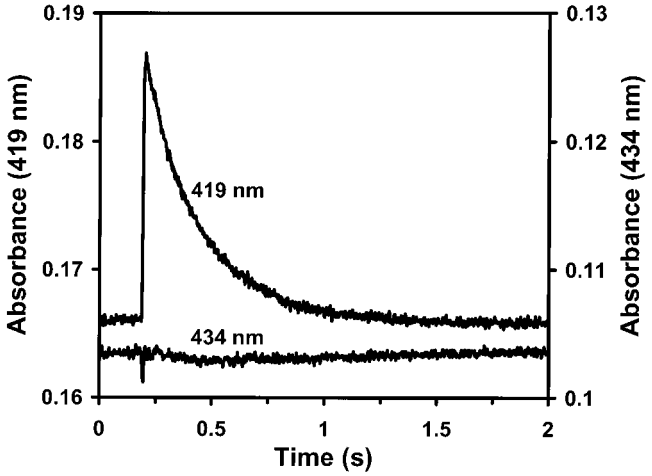

FIGURE 4: Reaction between 0.4 μM yCc^{II} and 0.5 μM CMPI prebound with 0.5 μM yCc^{III} in 5 mM sodium phosphate, pH 7.0, at 22 °C. The solid curve is the best fit to the first two lines of Scheme 2 with $k_d = 5.1 \pm 1$ s^{-1}. No absorbance change was observed at 434 nm.

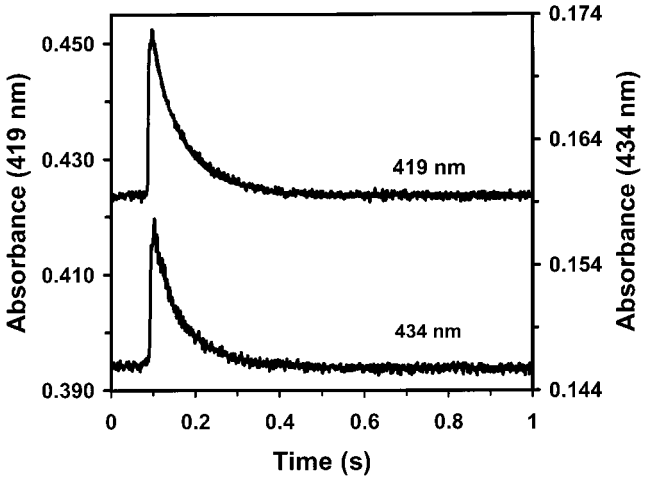

FIGURE 5: Reaction between 3 μM yCc^{II} and 0.42 μM CMPI(MI) in 5 mM sodium phosphate buffer, pH 7.0, at 22 °C. The 419 and 434 nm transients were fitted to Scheme 1 with $k_d = 19 \pm 4$ s^{-1}.

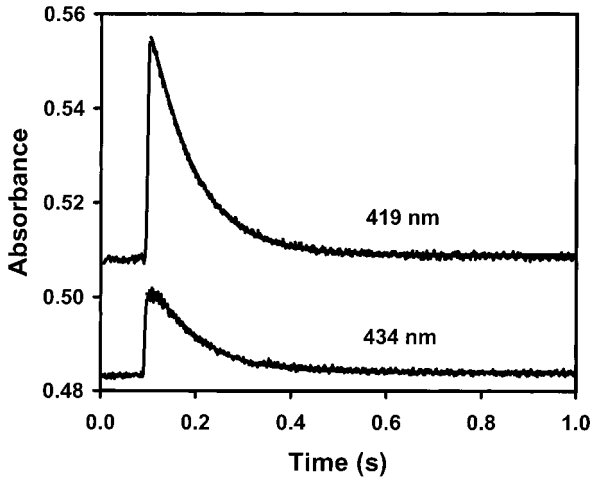

FIGURE 6: Reaction between 3 μM yCc^{II} and 0.5 μM CMPI(MI) prebound with 0.5 μM yCc^{III} in 5 mM sodium phosphate buffer, pH 7.0, at 22 °C. The 419 and 434 nm transients were fitted to Scheme 2 with $k_d = 25 \pm 5$ s^{-1}.

corresponding to the reaction of 0.4 μM yCc^{II} with 0.4 μM radical cation in CMPI. No 434 nm transient was observed, indicating that no oxyferryl heme was reduced. Since only the radical cation is reduced in this experiment, the inherent rate constant for reduction of the radical cation must be much larger than for reduction of the oxyferryl heme, as previously observed in ruthenium experiments (*19*). The k_{obs} value for reduction of the radical cation in the preformed complex (Figure 4) is the same as for reduction of oxyferryl heme in the experiment of Figure 3, consistent with a mechanism involving rate-limiting dissociation of yCc^{III}.

The complete reduction of CMPI by 2 equiv of Cc^{II} requires at least two complex formation and dissociation steps and two intracomplex electron-transfer steps, as shown in Scheme 1. The formation and dissociation rate constants, k_f and k_d, are assumed to be independent of the redox state of Cc. The validity of this assumption is supported by the results of McLendon et al. (*41*) that the equilibrium dissociation constant K_d for the high-affinity binding site on MgCcP is the same for yCc^{II} and yCc^{III} and of Mauk et al. (*42*) that the dissociation constant for native CcP differed by only a factor of 2 for oxidized and reduced yCc. The transients of Figure 3 were fitted to the complete mechanism of Scheme 1 using numerical integration methods, assuming that the intracomplex electron-transfer rate constants were the same as measured with yeast Ru-39-Cc, $k_{eta} = 2 \times 10^6$ s^{-1} and $k_{etb} = 5000$ s^{-1} (*19*). It was also assumed that the complex formation rate constant k_f was greater than 10^9 M^{-1} s^{-1}, as shown in the experiment of Figure 2. The fits did not depend on the values of k_{eta}, k_{etb}, and k_f as long as $k_{eta} > 1000$ s^{-1}, $k_{etb} > 1000$ s^{-1}, and $k_f > 10^9$ M^{-1} s^{-1}. Under these conditions, the rate-limiting step in the reduction of the oxyferryl heme is k_d, the rate constant for dissociation of the II·Cc^{III} complex. The solid lines in Figure 3 are the best fits to the 419 and 434 nm transients with $k_d = 4.7 \pm 1$ s^{-1}. The transients of Figure 4 were fitted to the mechanism shown in the first two lines of Scheme 2, which involves the reaction of 1 equiv of Cc^{II} with the preformed CMPI·Cc^{III} complex. The solid curve gives the best fit with $k_d = 5.1 \pm 1$ s^{-1}. The values of k_d for the experiments of Figures 3 and 4 are the same, consistent with rate-limiting dissociation of yCc^{III} from the high-affinity site.

To study the role of the low-affinity site, the reaction between excess yCc^{II} and CMPI was studied in the presence and absence of bound yCc^{III}. Figure 5 shows the reaction between 3 μM yCc^{II} and 0.42 μM CMPI in 5 mM sodium phosphate. The k_{obs} values for both the 434 and 419 nm transients are 11 s^{-1}. The amplitude of the 434 nm transient accounted for reduction of 0.42 μM oxyferryl heme, while the 419 nm transient corresponded to the reduction of 0.42 μM oxyferryl heme by 0.42 μM Cc^{II}. The initial reduction of the Trp-191 radical cation by yCc^{II} was too fast to be resolved by the stopped-flow spectrophotometer. The solid lines are the best fits of Scheme 1 to the transients with $k_d = 19 \pm 4$ s^{-1}. Figure 6 shows the reaction of 3 μM yCc^{II} with 0.5 μM preformed CMPI·yCc^{III} complex in 5 mM sodium phosphate. The k_{obs} values of the 419 and 434 nm transients were both 10.5 s^{-1}. The amplitude of the 434 nm transient accounts for the reduction of 0.5 μM oxyferryl heme, while the amplitude of the 419 nm transient corresponds to the reaction of 1.0 μM yCc^{II} with 0.5 μM CMPI. Therefore, the reduction of both the Trp-191 radical cation

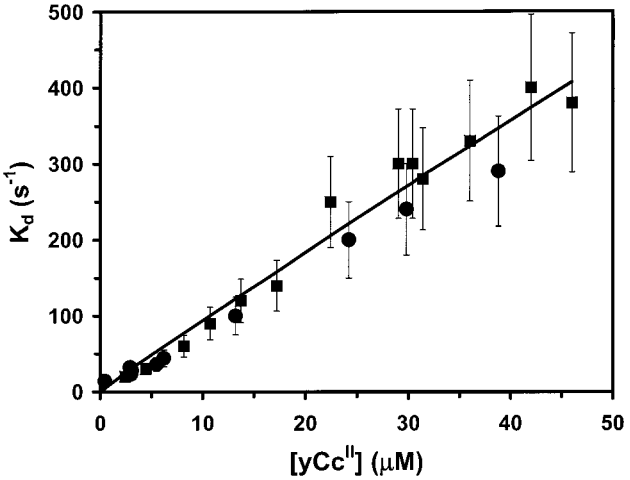

FIGURE 7: Effect of yCc^{II} concentration on the apparent dissociation rate constant k_d. The reaction between 1−50 μM yCc^{II} and 0.5 μM CMPI with 0.5 μM prebound yCc^{III} was carried out in 5 mM sodium phosphate buffer, pH 7.0, at 22 °C. The k_d values obtained by fitting the 419 and 434 nm transients as shown in Figure 6 were fitted to eq 1 by nonlinear regression with $k_d < 5$ s^{-1}, $k_{d2} \geq 2000$ s^{-1}, $K_{d2} \geq 200$ μM, and $k_{d2}/K_{d2} = (1 \pm 0.3) \times 10^7$ M^{-1} s^{-1}. Symbols: (■) wild-type yeast CcP; (●) CcP(MI).

Scheme 3

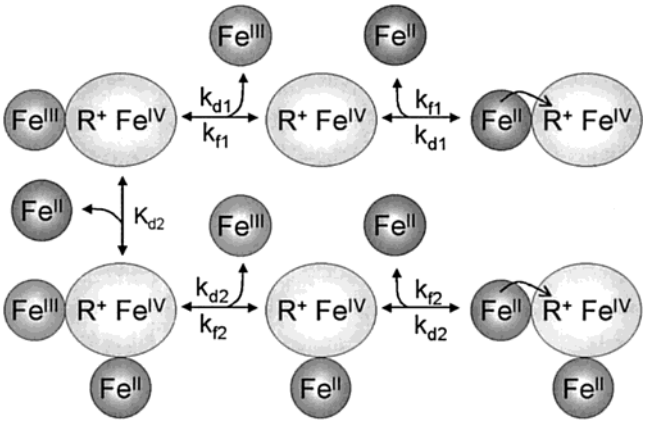

and the oxyferryl heme is resolved in this experiment. The solid curves are the best fits of Scheme 2 to the 419 and 434 nm transients with $k_d = 25 \pm 5$ s^{-1}. The lag phase in the 434 nm transient is due to the initial reduction of the Trp-191 radical cation, which does not change the 434 nm absorbance. After the initial lag phase, the oxyferryl heme is reduced at the same rate as the radical cation, and both are rate-limited by the same dissociation constant k_d. Furthermore, the value of k_d is the same as in the experiment of Figure 5, which does not include bound yCc^{III}. The value of k_d increases nearly linearly with increasing concentrations of yCc^{II} (Figure 7). The rate constants for reduction of the Trp-191 radical cation and oxyferryl heme remain the same at all concentrations of yCc^{II}, consistent with a mechanism involving rate-limiting dissociation of yCc^{III}. The concentration dependence of k_d was fitted to a "substrate-induced product dissociation" mechanism, in which it is assumed that the binding of yCc^{II} to a second low-affinity site increased the rate constant for dissociation of yCc^{III} from the high-affinity site (Scheme 3). For simplicity, this scheme shows just the first step in reduction of CMPI, the reduction of the radical cation. The same scheme is used for reduction of

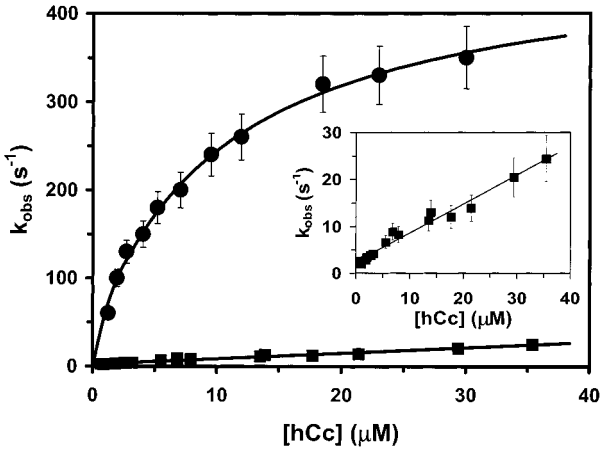

FIGURE 8: Reaction of hCc^{II} with CMPI in the presence and absence of yCc^{III} bound to the high-affinity site. (●) Reaction between 1−30 μM hCc^{II} and 0.5 μM CMPI in 5 mM sodium phosphate buffer, pH 7.0, at 22 °C. The values of k_{obs} were determined from the 419 and 434 nm transients. The solid line is the best fit to the equation $k_{obs} = k_{cat}[hCc]/(K_m + [hCc])$ with $k_{cat} = 470 \pm 100$ s^{-1} and $K_m = 8 \pm 2$ μM. (■) Reaction between 1−40 μM hCc^{II} and 0.5 μM preformed CMPI·yCc^{III} complex in 5 mM sodium phosphate buffer, pH 7.0, at 22 °C. The inset shows these data on an expanded scale. The solid line is simply a straight line through the k_{obs} values.

the oxyferryl heme in CMPII. The apparent dissociation rate constant k_d for the mechanism of Scheme 3 is given by

$$k_d = k_{d1}K_{d2}/([yCc^{II}] + K_{d2}) + k_{d2}[yCc^{II}]/([yCc^{II}] + K_{d2}) \quad (1)$$

where k_{d1} is the true rate constant for dissociation of yCc^{III} from the high-affinity binding site when the low-affinity site is not occupied, k_{d2} is the rate constant for dissociation of yCc^{III} from the high-affinity site when the low-affinity site is occupied, and K_{d2} is the equilibrium dissociation constant for the low-affinity site. The data of Figure 7 were fit to eq 1 with $k_{d1} < 5$ s^{-1}, $k_{d2} \geq 2000$ s^{-1}, $K_{d2} \geq 200$ μM, and $k_{d2}/K_{d2} = (1 \pm 0.3) \times 10^7$ M^{-1} s^{-1}. Because of the small hyperbolic curvature in the data of Figure 7, the individual values of k_{d2} and K_{d2} could not be obtained accurately. Under these conditions where $K_{d2} \gg [yCc^{II}]$, eq 1 simplifies to

$$k_d = k_{d1} + k_{d2}[yCc^{II}]/K_d \quad (2)$$

The data of Figure 7 were fitted to eq 2 with $k_d < 5$ s^{-1} and $k_{d2}/K_{d2} = (1 \pm 0.3) \times 10^7$ M^{-1} s^{-1}. The reaction of yCc with recombinant CcP(MI) was found to be the same within experimental error as the reaction with wild-type yeast CcP (Figure 7). Likewise, there were no significant differences between the two CcP preparations in the experiments of Figures 2−6 (data not shown).

Reaction of Horse Cc^{II} with CMPI and the CMPI·yCc^{III} Complex. The role of the low-affinity site was further explored using horse Cc, which is known to bind much more weakly to CcP than yCc (*25*, *41*). The reaction between 1.2 μM hCc^{II} and 0.5 μM CMPI was similar to that involving yCc^{II}. The initial reduction of the Trp-191 radical cation was too fast to resolve in the stopped flow, while the reduction of the oxyferryl heme was completely resolved with a k_{obs} of 40 s^{-1}. The value of k_{obs} increased with increasing hCc^{II} concentration to 350 s^{-1} at 30 μM hCc^{II} (Figure 8). The concentration dependence data were fitted to a simple

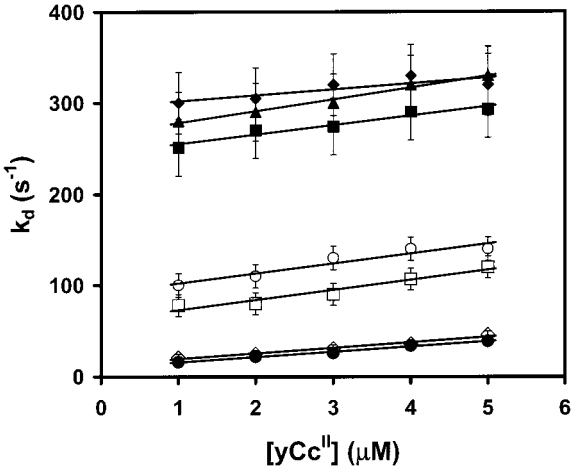

FIGURE 9: Effect of CcP surface mutants on the apparent dissociation rate constant k_d. Experiments were carried out between 1−5 μM yCc^{II} and 0.5 μM CMPI in 5 mM sodium phosphate, pH 7.0, and 20 mM NaCl at 22 °C. The 419 and 434 nm transients were fitted to Scheme 1 to obtain apparent k_d values. The solid lines are the best fits to eq 2 with the k_{d1} and k_{d2}/K_{d2} values shown in Table 1. Symbols: (◇) CcP(MI), (□) E32Q, (◆) D34N, (○) E35Q, (■) E290N, (●) E291Q, and (▲) A193F.

Michaelis−Menten equation with $k_{cat} = 470$ s^{-1} and $K_m = 8$ μM. The reaction of hCc^{II} with CMPI was greatly inhibited by prebinding 1 equivt of yCc^{III} to the high-affinity site (Figure 8). Mixing 0.5 μM hCc^{II} with 0.5 μM preformed CMPI·yCc^{III} complex resulted in reduction of the radical cation with a k_{obs} value of 1.7 s^{-1} and no reduction of the oxyferryl heme. When excess hCc^{II} was mixed with 0.5 μM CMPI·yCc^{III}, the radical cation was initially reduced, followed by reduction of the oxyferryl heme with the same rate constant. The value of k_{obs} increased nearly linearly to only 25 s^{-1} as the concentration of hCc^{II} was increased to 35 μM (Figure 8). These results are consistent with a mechanism in which the CMPI·yCc^{III} complex must first dissociate before hCc^{II} can bind and react at the high-affinity site. Because of the much higher affinity of yCc^{III}, this process is very slow, even at high concentrations of hCc^{II}. The same kinetic parameters were observed for both wild-type CcP and recombinant CcP(MI).

Effect of CcP Surface Mutations on the Reaction between yCc^{II} and CMPI. The effects of the CcP surface mutants E32Q, E35Q, D34N, E290N, and A193F on the reaction between yCc^{II} and CMPI were studied in 5 mM sodium phosphate, pH 7.0, and 20 mM NaCl. At this ionic strength the dissociation rate constant k_{d1} for wild-type CcP increases to a measurable value of 13 s^{-1}, and the effects of the low-affinity site become smaller (*20*). The apparent dissociation rate constant k_d was measured by numerical integration fits of Scheme 1 to the 419 and 434 nm transients as described above. Regression analysis of the k_d values obtained with [yCc^{II}] concentrations of 1−5 μM using eq 2 yielded $k_{d1} = 13 \pm 2$ s^{-1} and $k_{d2}/K_{d2} = (7.5 \pm 2) \times 10^6$ M^{-1} s^{-1} for wild-type CcP (Figure 9, Table 1). Low concentrations of yCc^{II} (1−5 μM) were used to optimize measurement of k_{d1}. The k_{d1} values of the D34N, E290N, A193F, E35Q, and E32Q mutants were 22-, 19-, 21-, 7-, and 5-fold larger than the CcP(MI) control at 30 mM ionic strength, while the E291Q mutation has essentially no effect on k_{d1} (Figure 9, Table 1). These results indicate that alteration of E32, D34, E35, E290, or A193 at the Pelletier−Kraut binding site significantly increases the dissociation rate constant of the high-affinity complex.

Table 1: Effect of CcP Surface Mutants on the Reaction with yCc[a]

CcP mutant	k_{d1} (s^{-1})	k_{d2}/K_{d2} (10^6 M^{-1} s^{-1})	k_{second} (10^6 M^{-1} s^{-1})
CcP(MI)	13 ± 3	8 ± 2	50 ± 10
E32Q	63 ± 10	14 ± 3	50 ± 10
E34N	290 ± 40	10 ± 2	9 ± 2
E35Q	91 ± 10	15 ± 3	25 ± 5
E290N	250 ± 40	15 ± 3	20 ± 4
E291Q	11 ± 3	7 ± 2	50 ± 10
A193F	270 ± 40	16 ± 3	20 ± 4

[a] The reaction at low ionic strength was carried out by mixing 1−5 μM yCc^{II} with the 0.5 μM CMPI mutant in 20 mM NaCl and 5 mM sodium phosphate buffer, pH 7.0, at 22 °C. The concentration dependence of the apparent dissociation rate constant k_d measured in Figure 9 was fitted to eq 2 by regression analysis to determine k_{d1} and k_{d2}/K_{d2}. The second-order rate constant k_{second} for the reaction between yCc^{II} and the oxyferryl heme was measured at high ionic strength in 5 mM phosphate, pH 7.0, and 300 mM NaCl at 22 °C (*17*).

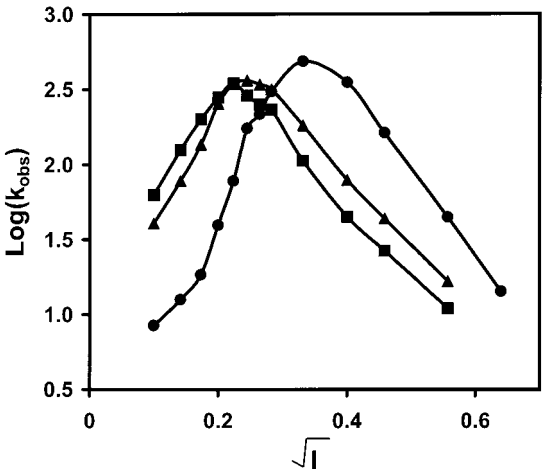

FIGURE 10: Effect of ionic strength on k_{obs} (s^{-1}) for the reaction between excess yCc^{II} and the oxyferryl heme in CMPI mutants. The reaction was carried out with 3 μM yCc^{II} and 0.5 μM CMPI in 5 mM sodium phosphate, pH 7.0, and 0−600 mM NaCl at 22 °C. Symbols: (●) CcP(MI), (■) D34N, and (▲) E290N. The solid lines simply connect the points.

The effect of ionic strength on the reaction between yCc^{II} and CMPI mutants was also studied. The rate constant k_{obs} for the reaction between 3 μM yCc^{II} and 0.5 μM wild-type CMPI increased from 10 s^{-1} at 10 mM ionic strength to a maximum of 300 s^{-1} at 125 mM ionic strength and then decreased to 5 s^{-1} at 600 mM ionic strength (Figure 10). k_{obs} is controlled by the rate constant for dissociation of the high-affinity complex, k_{d1}, at low ionic strength, and increasing ionic strength increases k_{d1}. Above 125 mM ionic strength, the high-affinity complex is dissociated, and k_{obs} is controlled by the complex formation rate constant k_f. Further increases in ionic strength decrease k_f (Figure 10) (*20*). The value of k_{obs} for the D34N and E290N mutants is much larger than that of wild-type CcP at 5 mM ionic strength and increases to a maximum at a lower ionic strength, indicating that the high-affinity complex is weaker for these mutants, and dissociates at a lower ionic strength. The value of k_{obs} is smaller for D34N and E290N at high ionic strength, indicating that these mutations decrease the value of k_f (Figure 10).

DISCUSSION

The presence of both low- and high-affinity Cc binding sites on CcP has greatly complicated elucidation of the complete mechanism of the enzyme. Direct equilibrium binding studies have shown that yCc binds to CcP to form a high-affinity 1:1 complex with a dissociation constant K_d of less than 0.1 μM at 10 mM ionic strength (*25*, *26*, *41*). A second molecule of yCc can then bind to form a 2:1 complex with much lower affinity (*25*, *26*, *35*). The steady-state reaction of yCc^{II} with CMPI is extremely slow at yCc^{II} concentrations which should saturate the high-affinity binding site (*21*, *25*, *28*, *29*). The steady-state velocity has a hyperbolic dependence on the concentration of yCc^{II}, with a large K_m value characteristic of the low-affinity binding site (*21*, *25*, *28*, *29*). Thus, enzyme turnover at low ionic strength is controlled by yCc binding to the low-affinity site. Similar results have been observed for the reduction of the oxyferryl heme in CMPI by excess yCc^{II} under single-turnover conditions (*22*). A critical question is whether the low-affinity binding site is active in electron transfer to the oxyferryl heme (*33*, *35*) or instead promotes the dissociation of the high-affinity product complex (*20*). To address the role of the low-affinity site, we have studied the reaction between yCc^{II} and CMPI in the presence and absence of yCc^{III} bound to the high-affinity site.

The reaction between 1.1 μM yCc^{II} and 0.4 μM CMPI at 10 mM ionic strength involves rapid reduction of the Trp-191 radical cation with a rate constant that is too large to resolve in the stopped-flow spectrophotometer, followed by slow reduction of the oxyferryl heme with a rate constant of 3.6 s^{-1} (Figure 3). In contrast, the reaction between 0.4 μM yCc^{II} and a preformed complex between 0.5 μM yCc^{III} and 0.5 μM CMPI involves slow reduction of the radical cation with a rate constant of 3.5 s^{-1} (Figure 4). Since only the radical cation is reduced in this experiment, the inherent rate constant for reduction of the radical cation must be much larger than that for reduction of the oxyferryl heme. This is consistent with previous measurements of $k_{eta} = 2 \times 10^6$ s^{-1} and $k_{etb} = 5000$ s^{-1} for the reaction of Ru-39-yCc with CMPI at the high-affinity binding site (*19*). Moreover, the observed rate constant for reduction of the radical cation in the preformed complex (Figure 4) is the same as for reduction of the oxyferryl heme (Figure 3), consistent with a mechanism involving rate-limiting dissociation of the product complex $CMPII{\cdot}yCc^{III}$. The kinetics shown in Figures 3 and 4 were fitted to Schemes 1 and 2, respectively, with $k_d = 5 \pm 1$ s^{-1}, $k_f > 10^9$ M^{-1} s^{-1}, $k_{eta} > 1000$ s^{-1}, and $k_{etb} > 1000$ s^{-1}.

The reaction of excess yCc^{II} with a preformed 1:1 complex between yCc^{III} and CMPI involves initial reduction of the Trp-191 radical, followed by reduction of the oxyferryl heme with the same observed rate constant (Figure 6). The rate constant increased nearly linearly with increasing yCc^{II} concentrations, with only a slight hyperbolic curvature (Figure 7). Essentially the same concentration dependence was previously observed for the reaction between yCc^{II} and CMPI (*22*, *29*) at low ionic strength and also for the steady-state reaction (*21*, *28*, *29*). It is generally agreed that this phase of the reaction is associated with the low-affinity binding site with a dissociation constant K_d of approximately 200 μM (*21*, *22*), consistent with measurements using other techniques (*25*, *35*). A key finding in the present study is that the k_{obs} values for reduction of the Trp-191 radical cation and the oxyferryl heme in the preformed 1:1 $CMPI{\cdot}yCc^{III}$ complex are the same over the entire concentration range of yCc^{II} (Figures 6 and 7). In principle, this behavior could involve a mechanism involving direct rate-limiting electron transfer from yCc^{II} in the low-affinity site to the oxyferryl heme in $CMPI(Fe^{IV},R^{\bullet+})$ to form $CMPII(Fe^{III},R^{\bullet+})$, followed by rapid internal electron transfer to form $CMPII(Fe^{IV}{=}O,R)$. However, this mechanism is inconsistent with the observation that several different reductants reacting at different sites on CMPI all reduce the radical cation with a larger rate constant than the oxyferryl heme. First, Ru-39-Cc binding in the high-affinity site reduces the radical cation 400-fold more rapidly than the oxyferryl heme (*19*). Second, mesidine and other anilines reduce the radical cation 4.2-fold more rapidly than the oxyferryl heme even though there is evidence that they react near the δ-meso edge of the heme on the opposite side from Trp-191 (*43*, *44*). Third, ferrocyanide reduces the radical cation 3.2-fold more rapidly than the oxyferryl heme but reacts at a site different from the high-affinity Cc site, possibly near the δ-meso edge of the heme (*6*, *45*, *46*). Thus, reduction of the Trp-191 radical cation is inherently more rapid than that of the oxyferryl heme even when the electron originates from the opposite side of the heme. Reduction of the oxyferryl heme is a complex process involving proton transfer to the oxygen and release of water and is inherently slower than reduction of the radical cation (*19*). Therefore, since the k_{obs} values for reduction of the radical cation and the oxyferryl heme in the preformed 1:1 $CMPI{\cdot}yCc^{III}$ complex are the same, they must be rate-limited by some step other than electron transfer. A mechanism involving rate-limiting dissociation of the $CMPI{\cdot}yCc^{III}$ product complex as shown in Schemes 1 and 2 is most consistent with a wide range of observations. It is proposed that binding yCc^{II} to the low-affinity site increases the rate constant for dissociation of yCc^{III} from the high-affinity site, as shown in Scheme 3. This is a "substrate-assisted product dissociation" mechanism similar to those proposed by other workers (*41*, *47*−*49*). The kinetic parameters obtained for the data of Figure 7 are $k_{d1} < 5$ s^{-1}, $k_{d2} \geq 2000$ s^{-1}, $K_{d2} \geq 200$ μM, and $k_{d2}/K_{d2} = (1 \pm 0.3) \times 10^7$ M^{-1} s^{-1}. Although the value of K_{d2} was not determined accurately because of the small curvature in the data of Figure 7, it is consistent with measurements of the dissociation constant of the low-affinity binding site by other techniques (*21*, *25*, *28*, *29*).

It is well-established that hCc binds much more weakly to the high-affinity site than yCc but that hCc and yCc bind with similar affinities to the low-affinity site (*25*, *32*, *35*, *41*). This property was utilized in a study of the reaction of hCc^{II} with a preformed 1:1 complex in which yCc^{III} is bound strongly to the high-affinity site in CMPI (Figure 8). The reaction of hCc^{II} with the $CMPI{\cdot}yCc^{III}$ complex is greatly inhibited compared to the reaction of hCc with CMPI (Figure 8) or the reaction of yCc^{II} with the preformed $CMPI{\cdot}yCc^{III}$ complex (Figure 7). The k_{obs} values for reduction of the radical cation and the oxyferryl heme are the same over the entire hCc^{II} concentration range, consistent with a mechanism in which hCc^{II} binding to the low-affinity site increases the rate of dissociation of yCc^{III} from the high-affinity site, as shown in Scheme 3. The very small rate observed for the reaction of hCc^{II} with the $CMPI{\cdot}yCc^{III}$ complex, even when

hCc^{II} is in large excess over yCc^{III}, is due to the much lower affinity of hCc^{II} for the high-affinity site than that of yCc^{III}. Equilibrium binding studies have shown that yCc binds to the high-affinity site more than 100-fold more strongly than hCc (*41*, *50*). The concentration dependence of k_{obs} shown in Figure 8 is consistent with a K_{d2} value of 200 μM or greater, which is comparable to a K_{d2} value of 130 μM determined for zinc hCc binding to the low-affinity site at 4.5 mM ionic strength (*31*). The same value of K_{d2} was obtained for zinc hCc when the high-affinity site was occupied by copper Cc from the fungus *Pichia membranefaciens*, indicating that the interaction with the low-affinity site does not depend on whether the high-affinity site is occupied by a tight-binding fungal Cc or weak-binding hCc (*32*). The finding that reduction of oxyferryl heme by hCc^{II} is greatly inhibited by binding yCc^{III} to the high-affinity site (Figure 8) provides strong evidence that this reaction involves electron transfer from the high-affinity binding site rather than the low-affinity site as suggested by others (*33*, *35*).

The effects of ionic strength and CcP surface charge mutations are also consistent with the mechanism of Schemes 1 and 3. The rate constant k_{obs} for wild-type CMPI increased to a maximum at 125 mM ionic strength and then decreased with further increases in ionic strength (Figure 10). k_{obs} is thus controlled by dissociation of the high-affinity product complex at low ionic strength and by complex formation at high ionic strength. The CcP surface mutations D34N, E290N, A193F, E35Q, and E32Q increase k_{obs} by up to 20-fold at low ionic strength, which was shown to result from an increase in the rate constant k_{d1} for dissociation of the high-affinity complex (Figure 9, Table 1). The effects of these mutations in the Pelletier−Kraut high-affinity binding domain provide additional evidence that dissociation of the high-affinity product complex is rate-limiting at low ionic strength. These same CcP surface mutations decrease k_{obs} at high ionic strength (*17*), consistent with a decrease in the value of the complex formation rate constant k_f. These results indicate that the high-affinity binding site is involved in electron transfer at all ionic strengths. The low-affinity binding site becomes too weak to play a role in the reaction at ionic strengths above 70 mM and is therefore not involved under physiological conditions (*20*, *21*).

Recombinant CcP(MI) used in previous studies from this laboratory and others has two variations in sequence compared to wild-type yeast CcP, D152G and T53I (*36*, *37*, *51*). It has been suggested that these sequence differences may affect the interaction of yCc with the low-affinity site, since residue 152 is close to the proposed location of the low-affinity binding site (*34*). However, there were no significant differences in the kinetics of CcP(MI) and wild-type CcP in the experiments of Figures 2−8, indicating that these mutations do not affect the interaction of yCc with the low-affinity binding site. Likewise, no significant differences were observed between wild-type yeast CcP and CcP(MI) in the reactions with Cc at high ionic strength (*15*−*17*).

On the basis of Brownian dynamics simulations, Northrup et al. (*52*) suggested that the low-affinity binding site might be located near Asp-148, which is distant from the high-affinity binding site but close to the heme. This is supported by the finding that the mutation K149E increases the affinity of zinc hCc for the low-affinity binding site by 6-fold (*34*). To test the role of this binding site in electron transfer, Papa et al. (*53*) prepared a 1:1 yCc·CcP cross-linked complex in which a disulfide bond was formed between yCc Cys-79 and CcP Cys-149. The rate constant for electron transfer from yCc^{II} to CMPI in the complex was only 1 s^{-1} and involved reduction of the radical cation rather than the oxyferryl heme, even though the tethered yCc is closer to the CcP heme than to Trp-191 (14−18 versus 20−23 Å). The steady-state kinetics of this complex with solution phase yCc^{II} or hCc^{II} was similar to that of wild-type CcP, calling into question the assignment of the low-affinity site to the region near Asp-148. Another complex in which yCc was cross-linked to the high-affinity site in CcP was found to have a turnover number for the reaction with solution phase yCc^{II} that was less than 10% of the value for native CcP (*53*). The results with these cross-linked complexes provide additional evidence that electron transfer from the low-affinity site to the oxyferryl heme is much slower than from the high-affinity site.

A comparison of the electron-transfer properties of the radical cation and oxyferryl heme in CMPI with the results of Hoffman and co-workers using zinc-substituted Cc or CcP (*30*−*35*) provides important insight into the nature of biological electron transfer. They found that ^{3}Zn-hCc bound in the low-affinity site transfers an electron to the ferric heme in CcP with a rate constant of 1490 s^{-1} but is nearly inactive in electron transfer from the high-affinity site (*31*). The Trp-191 indole cannot be oxidized to the radical cation by the reductive ^{3}Zn-porphyrin and cannot be a redox intermediate in the reaction. Hence, the large separation between the ^{3}Zn-hCc in the high-affinity site and the CcP heme (26.5 Å, metal to metal) would limit the rate of electron transfer. ^{3}Zn-hCc binding in the low-affinity site is closer to the CcP heme (22−25 Å, metal to metal), consistent with the larger rate of electron transfer. Reduction of the CcP ferric heme by ^{3}Zn-hCc is a pure electron-transfer process which should be governed by Marcus theory. In contrast, reduction of the oxyferryl heme is a complex process involving proton transfer to the oxygen atom and release of water and is inherently slower than a simple electron-transfer process. We have provided evidence that reduction of CMPII(Fe^{IV}=O,R) involves rapid internal electron transfer leading to transient formation of the radical cation in CMPII(Fe^{III},$R^{\bullet+}$), which is then reduced by yCc^{II} in the high-affinity binding site (*18*, *19*). Because the radical cation is a redox intermediate in electron transfer, the effective distance of electron transfer is much less (16 Å from the yCc heme edge to the Trp-191 indole) and the rate can be much faster. It is well-established that biological electron transfer is greatly accelerated by the presence of redox intermediates with smaller separations (*54*). The reduction of the oxyferryl heme thus requires transient formation of the Trp-191 radical cation as an essential intermediate. The critical role of the Trp-191 radical cation was demonstrated by the finding that the rate of reduction of the oxyferryl heme by yCc^{II} was decreased more than 10000-fold by mutating Trp-191 to Phe (*6*). The very small rate of reduction of the oxyferryl heme from the low-affinity binding site most likely reflects the large distance between this site and Trp-191 and the absence of an efficient pathway for electron transfer. The distance between Trp-191 and the yCc heme at the proposed low-affinity binding site near Asp-148 has been estimated to be 20−23 Å, which would result in a very small rate of electron transfer (*53*). However, the

location of the low-affinity site remains uncertain and may even involve a distribution of sites (*34*, *53*).

REFERENCES

1. Marcus, R. A., and Sutin, N. (1985) *Biochim. Biophys. Acta 811*, 265−322.
2. Moser, C. C., Keske, J. M., Warncke, K., Farid, R. S., and Dutton, P. L. (1992) *Nature 355*, 796−802.
3. Davidson, V. L. (2000) *Acc. Chem. Res. 33*, 87−93.
4. Pelletier, H., and Kraut, J. (1992) *Science 258*, 1748−1755.
5. Millett, F., Miller, M. A., Geren, L., and Durham, B. (1995) *J. Bioenerg. Biomembr. 27*, 341−351.
6. Mauro, J. M., Fishel, L. A., Hazzard, J. T., Meyer, T. E., Tollin, G., Cusanovich, M. A., and Kraut, J. (1988) *Biochemistry 27*, 6243−6256.
7. Scholes, C. P., Liu, Y., Fishel, L. A., Farnum, M. F., Mauro, J. M., and Kraut, J. (1989) *Isr. J. Chem. 29*, 85−92.
8. Erman, J. E., Vitello, L. B., Mauro, J. M., and Kraut, J. (1989) *Biochemistry 28*, 7992−7995.
9. Sivaraja, M., Goodin, D. B., Smith, M., and Hoffman, B. M. (1989) *Science 245*, 738−740.
10. Miller, M. A., Han, G. W., and Kraut, J. (1994) *Proc. Natl. Acad. Sci. U.S.A. 91*, 11118−11122.
11. Fitzgrald, M. M., Churchill, M. J., McRee, D. E., and Goodin, D. B. (1994) *Biochemistry 33*, 3807−3818.
12. Huyett, J. E., Doan, P. E., Gurbiel, R., Houseman, A. L. P., Sivaraja, M., Goodin, D. B., and Hoffman, B. M. (1995) *J. Am. Chem. Soc. 117*, 9033−9041.
13. Geren, L. M., Hahm, S., Durham, B., and Millett, F. (1991) *Biochemistry 30*, 9450−9457.
14. Hahm, S., Durham, B., and Millett, F. (1992) *Biochemistry 31*, 3472−3477.
15. Hahm, S., Geren, L., Durham, B., and Millett, F. (1993) *J. Am. Chem. Soc. 115*, 3372−3373.
16. Hahm, S., Miller, M. A., Geren, L., Kraut, J., Durham, B., and Millett, F. (1994) *Biochemistry 33*, 1473−1480.
17. Miller, M. A., Liu, R.-Q., Hahm, S., Geren, L., Hibdon, S., Kraut, J., Durham, B., and Millett, F. (1994) *Biochemstry 33*, 8686−8693.
18. Liu, R.-Q., Hahm, S., Miller, M. A., Han, G. W., Geren, L., Hibdon, S., Kraut, J., Durham, B., and Millett, F. (1994) *Biochemistry 33*, 8678−8685.
19. Wang, K., Mei, H., Geren, L., Miller, M. A., Saunders, A., Wang, X., Waldner, J. L., Pielak, G. J., Durham, B., and Millett, F. (1996) *Biochemistry 35*, 15107−15119.
20. Mei, H., Wang, K., McKee, S., Wang, X., Waldner, J. L., Pielak, G. J., Durham, B., and Millett, F. (1996) *Biochemistry 35*, 15800−15806.
21. Miller, M. A. (1996) *Biochemistry 35*, 15791−15799.
22. Matthis, A. L., Vitello, L. B., and Erman, J. E. (1995) *Biochemistry 34*, 9991−9999.
23. Nuevo, M. R., Chu, H.-H., Vitello, L. B., and Erman, J. E. (1993) *J. Am. Chem. Soc. 115*, 5873−5874.
24. Summers, F. E., and Erman, J. E. (1988) *J. Biol. Chem. 263*, 14,267−14,275.
25. Kang, C. H., Ferguson-Miller, S., and Margoliash, E. (1977) *J. Biol. Chem. 252*, 919−926.
26. Kornblatt, J. A., and English, A. M. (1986) *Eur. J. Biochem. 155*, 505−511.
27. Kim, K. L., Kang, D. S., Vitello, L. B., and Erman, J. E. (1990) *Biochemistry 29*, 9150−9159.
28. Matthis, A. L., and Erman, J. E. (1995) *Biochemistry 34*, 9985−9990.
29. Erman, J. E., Kang, D. S., Kim, D. L., Summers, F. E., Mathis, A. L., and Vitello, L. B. (1991) *Mol. Cryst. Liq. Cryst. 194*, 253−258.
30. Zhou, J. S., and Hoffman, B. M. (1993) *J. Am. Chem. Soc. 115*, 11008−11009.
31. Zhou, J. S., and Hoffman, B. M. (1994) *Science 265*, 1693−1696.
32. Zhou, J. S., Nocek, J. M., De Van, M. L., and Hoffman, B. M. (1995) *Science 269*, 204−207.
33. Zhou, J. S., Tran, S. T., McLendon, G., and Hoffman, B. M. (1997) *J. Am. Chem. Soc. 119*, 269−277.
34. Leesch, V. W., Bujons, J., Mauk, A. G., and Hoffman, B. M. (2000) *Biochemistry 39*, 10132−10139.
35. Stemp, E. D. A., and Hoffman, B. M. (1993) *Biochemistry 32*, 10848−10865.
36. Goodin, D. B., Davidson, M. G., Roe, J. A., Mauk, A. G., and Smith, M. (1991) *Biochemistry 30*, 4953−4962.
37. Fishel, L. A., Villafranca, J. E., Mauro, J. M., and Kraut, J. (1987) *Biochemistry 26*, 351−360.
38. Margoliash, E., and Frohirt, N. (1959) *Biochem. J. 71*, 570−575.
39. Coulson, A. G. W., Erman, J. E., and Yonetani, T. (1971) *J. Biol. Chem. 246*, 917−924.
40. Ho, P. S., Hoffman, B. M., Kang, C. H., and Margoliash, E. (1983) *J. Biol. Chem. 258*, 917−924.
41. McLendon, G., Zhang, Q., Wallin, S. A., Miller, R. M., Billstone, V., Spears, K. G., and Hoffman, B. M. (1993) *J. Am. Chem. Soc. 115*, 3665−3669.
42. Mauk, M. R., Ferrer, J. C., and Mauk, A. G. (1994) *Biochemistry 33*, 12609−12614.
43. Roe, J. A., and Goodin, D. B. (1993) *J. Biol. Chem. 268*, 20037−20045.
44. Wilcox, S. K., Jensen, G. M., Fitzgerald, M. M., McRee, D. E., and Goodin, D. B. (1996) *Biochemistry 35*, 4858−4866.
45. Jordi, H. C., and Erman, J. E. (1974) *Biochemistry 13*, 3734−3741.
46. DePillis, G. D., Sishta, B. P., Mauk, A. G., and Ortiz de Montellano, P. R. (1991) *J. Biol. Chem. 266*, 19334−19341.
47. Moench, S., Croni, S., Lou, B. S., Erman, J., and Satterlee, J. (1992) *Biochemistry 31*, 3663−3670.
48. Corin, A. F., Hake, R. A., McLendon, G., Hazzard, J. T., and Tollin, G. (1993) *Biochemistry 32*, 2756−2762.
49. Yi, Q., Erman, J. E., and Satterlee, J. D. (1994) *J. Am. Chem. Soc. 116*, 1981−1987.
50. Vitello, L. B., and Erman, J. E. (1987) *Arch. Biochem. Biophys. 258*, 621−629.
51. Miller, M. A., Geren, L., Han, G. W., Saunders, A., Beasley, J., Pielak, G. J., Durham, B., Millett, F., and Kraut, J. (1996) *Biochemistry 35*, 667−673.
52. Northrup, S. H., Boles, J. O., and Reynolds, J. C. L. (1988) *Science 241*, 67−70.
53. Pappa, H. S., Tajbaksh, S., Saunders, A. J., Pielak, G. J., and Poulos, T. L. (1996) *Biochemistry 35*, 4837−4845.
54. Page, C. C., Moser, C. C., Chen, X, and Dutton, P. L. (1999) *Nature 402*, 47−52.

BI016020A